Role of calcium on chloride binding in hydrated Portland cement – metakaolin – limestone blends

Zhenguo Shi[a], Mette Rica Geiker[b], Klaartje De Weerdt[b,c], Tone Anita Østnor[c], Barbara Lothenbach[d], Frank Winnefeld[d], Jørgen Skibsted[a*]

a. Department of Chemistry and Interdisciplinary Nanoscience Center (iNANO), Aarhus University, DK-8000 Aarhus C, Denmark

b. Department of Structural Engineering, Norwegian University of Science and Technology (NTNU), 7491 Trondheim, Norway

c. SINTEF Building and Infrastructure, 7491 Trondheim, Norway

d. Laboratory for Concrete & Construction Chemistry, Swiss Federal Laboratories for Materials Science and Technology (Empa), 8600 Dübendorf, Switzerland

[*] Corresponding author. Department of Chemistry and Interdisciplinary Nanoscience Center (iNANO), Aarhus University, DK-8000 Aarhus C, Denmark. Tel: +45-8715 5946; Fax: +45 8619 6199. E-mail address: jskib@chem.au.dk (J. Skibsted).

Abstract

Chloride binding is investigated for Portland cement – metakaolin – limestone pastes exposed to $CaCl_2$ and NaCl solutions. The phase assemblages and the amount of Friedel's salt are evaluated using TGA, XRD and thermodynamic modeling. A larger amount of Friedel's salt is observed in the metakaolin blends compared to the pure Portland cement. A higher total chloride binding is observed for the pastes exposed to the $CaCl_2$ solution relative to those in the NaCl solution. This is reflected by the fact that calcium increases the quantity of Friedel's salt in the metakaolin blends by promoting the transformation of strätlingite and/or monocarbonate to Friedel's salt. Calcium increases also the amount of chloride in the diffuse layer of the C-S-H for the pure cement. A linear correlation between the total bound chloride and the uptake of calcium from the $CaCl_2$ solution is obtained and found to be independent on the type of cement blend.

Keywords: Chloride (D); Metakaolin (D); pH (A); Calcium-Silicate-Hydrate (C-S-H) (B); Thermodynamic Calculations (B).

1 Introduction

Corrosion of steel reinforcement leads to loss of structural integrity and serviceability of reinforced concrete. An important contribution to this degradation is penetration of chloride ions from de-icing salt or sea water into reinforced concrete, which results in depassivation of the steel reinforcement when the chloride concentration exceeds a certain threshold level [1]. Attention to this problem has been paid for more than fifty years, during which significant research efforts have been made and several reviews have been published on this issue [2-5].

According to published studies, chloride ions in chloride exposed concrete are chemically bound in Friedel's salt ($Ca_4Al_2(OH)_{12}Cl_2 \cdot 4H_2O$) or present in the diffuse layer of the calcium-silicate-hydrate (C-S-H) phase, where both forms are often referred to as bound chloride. The remaining chloride ions are present in the pore solution, *i.e.*, as free chloride. One of the commonly used methods to evaluate the chloride resistance of concrete is to determine its chloride diffusion coefficient based on the total chloride profiles (*i.e.*, the total chloride content as function of the ingress depth), which is mainly affected by the pore structure [6, 7]. In addition to physical restrictions, several studies have also stated that chloride binding by the hydrated cement in concrete may affect the rate of chloride ingress [2, 8-11]. However, a recent study [12] has strongly indicated that chloride ions pass easily through the diffusion layer of the C-S-H. These findings from the literature underline the needs to further improve our knowledge on the different chloride binding mechanisms in order to assess the chloride resistance of concrete.

An efficient approach to enhance the chloride binding capacity of concrete is to partially replace Portland cement by alumina-rich supplementary cementitious materials (SCMs) [13-18], which are also beneficial for improvement of the pore structure [15, 19] and strength enhancement [19, 20] when an optimized replacement level is used. Heat-treated clay minerals represent a promising source of SCMs, as they are rich in alumina and silica. Furthermore, calcined clays receive increasing research interest because of their lower carbon footprint as compared to Portland cement and high abundance in the Earth's crust which make them attractive alternatives to industrial byproducts such as fly ash and slag. Limestone represents another type of SCM which is found to generate a synergetic effect with alumina-rich SCMs in blended Portland cements [21, 22]. The presence of such synergetic effects promotes the combined utilization of calcined clays (*e.g.* metakaolin) and limestone to replace Portland cement at high replacement levels without sacrificing the compressive strength of the resulting concrete [23, 24]. Significant research efforts have been devoted to the development and characterization of Portland cement – calcined clay – limestone blends, as recently summarized

in ref. [25]. The present work focuses on the chloride binding in Portland cement – metakaolin – limestone blends. A series of other durability investigations, *i.e.*, chloride ingress, carbonation and resistance to sulfate attack, have recently been presented for very similar blends [7, 26, 27].

The main contribution of alumina-rich SCMs on chloride binding is generally believed to be related to the alumina content of the mixture through formation of Friedel's salt. Very few studies focus on the chloride adsorption in the diffuse layer of the C-S-H phase in these blends, even though evidence for physical chloride binding on the surface of the C-S-H phase has been reported in several studies for synthetic C-S-H phases [28-30], hydrated Ca_3SiO_5 (C_3S) [31, 32], Portland cement [33], and silica fume – lime blends [34]. Because of the variations in composition and structure of the C-S-H phase, the physical chloride binding in the diffuse layer on the surface of the C-S-H becomes more complicated, which prevents the development of a reliable approach to evaluate its contribution to the measured total chloride binding, particular in blends with alumina-rich SCMs.

Several studies have also reported that the associated cations (*e.g.* Ca^{2+}) have a significant influence on chloride binding [17, 30, 32, 35-40]. A consistent conclusion from these investigations is that a higher total chloride binding is observed for samples exposed to $CaCl_2$ solutions as compared to NaCl solutions of the same chloride-ion concentration. The chloride binding has also been observed to increase with decreasing pH of the $CaCl_2$ exposure solutions with increasing chloride-ion concentration [32, 36, 37, 40, 41]. A linear relationship between the pH of the exposure solution (*i.e.*, for solutions of $MgCl_2$, $CaCl_2$ and NaCl) and the chloride binding has been established which is found to be independent of type of salt [37]. Based on this observation, it was concluded that the impact of different cations on the chloride binding is mainly governed by the pH of the exposure solution. However, it should be noted that these studies generally focused on synthetic C-S-H samples, hydrated C_3S and Portland cements whereas only a very few investigations have considered this effect for blends of Portland cement with SCMs. Thus, the conclusions, in particular for the pH dependency of the chloride binding, need to be verified for systems including SCMs. Furthermore, the driving force of the pH change on chloride binding should be analyzed in more detail to achieve a better understanding of the mechanisms of chloride binding.

The aim of this work is to investigate the impact of cations, Ca^{2+} vs. Na^{+}, on chloride binding in Portland cement – metakaolin – limestone blends. The total chloride binding isotherms are determined in order to evaluate the total chloride binding capacity of different blends exposed to NaCl and $CaCl_2$ solutions. The chloride binding in Friedel's salt is examined by data from

thermodynamic modeling and quantitative X-ray diffraction. The amount of chloride associated with the C-S-H phase is calculated by subtracting the amount of bound chloride in Friedel's salt from the total bound chloride determined by an equilibrium approach. The phase assemblages are analyzed by thermogravimetric analysis, X-ray diffraction and thermodynamic modelling. The pH values as well as the concentrations of chloride and calcium ions in the exposure solution are also determined. Based on these investigations, the role of calcium on chloride binding is assessed for Portland cement – metakaolin – limestone blends.

2 Experimental

The experimental setup, including preparation of the pastes, the exposure experiments and the analysis of the solids and solutions for obtaining the chloride binding isotherms, follows procedures described recently [37, 41].

2.1 Materials

The binders used in this study were made from a white Portland cement (wPc, CEM I 52.5 N), metakaolin (MK) and limestone (LS). The wPc was produced by Aalborg Portland A/S, Denmark, and included 3.1 wt.% LS, 4.1 wt.% gypsum and 1.9 % wt.% free lime. The MK was produced in the laboratory from kaolinite (Kaolinite Supreme^{TM}, Imerys Performance Minerals, UK) by thermal treatment in air at 550 ^{o}C for 20 h. The LS was a Maastrichtian chalk from Rørdal, Northern Denmark. The chemical compositions determined by X-ray fluorescence (XRF), the density and Blaine fineness for the starting materials are given in Table 1. The wPc contained 64.9 wt.% alite ("$3CaO{\cdot}SiO_2$": C_3S), 16.9 wt.% belite ("$2CaO{\cdot}SiO_2$": C_2S) and 7.8 wt.% calcium aluminate ($3CaO{\cdot}Al_2O_3$: C_3A). The content of the silicate phases were determined by ^{29}Si MAS NMR, assuming the Taylor compositions for these phases [42] and the quantity of the calcium aluminate phase by subsequent mass balance calculations. The small amount of iron is expected to be incorporated as guest ions in the alite, belite and C_3A phases. The salts, NaCl and $CaCl_2{\cdot}6H_2O$, of laboratory grade were dissolved in distilled water to prepare exposure solutions with the following chloride-ion concentrations: 0 (reference), 0.125, 0.25, 0.50, 1.0 and 2.0 mol/L. The actual concentrations were checked by titration prior to use.

2.2 Preparation of cement pastes

The binder compositions (Table 2) are the same as those used for mortars for carbonation experiments in another study [26]. The degrees of hydration for alite, belite and MK in

corresponding paste samples, measured by ^{29}Si MAS NMR, are summarized in Table 3 [43]. Three types of pastes (P, ML and M) as listed in Table 2 have been produced with the same water/binder ratio (w/b = 0.5) by mass. For each paste, deionized water was added to the cement blend and the paste was mixed (100 g blended cement + 50 g water for each mixing) by a motorized stirrer (Heidolph® RZR-2, Germany) equipped with a custom-made paddle (ø 45 mm). The mixing employed a rotational speed of 500 rpm for 3 minutes, then no rotation for 2 minutes, followed by mixing at 2000 rpm for 2 minutes, and the blend was then cast and sealed in a plastic bag. The fresh paste in the bags was flattened to a thickness of about 5 mm to facilitate the release of heat during hydration and avoid formation of hydration shells around the hydrating cement grains in order to maximize the degree of hydration [44]. For the same purpose of releasing heat during initial hydration, the pastes were sealed cured in a moist cabinet at 5 °C for the first three days followed by an additional curing in a moist room with relative humidity higher than 98% at 20 °C for about 2 months. Then the cement paste plates were crushed in a ceramic mortar to particles with a diameter of approximately 1 mm. The resulting powder was collected then in a one-liter polypropylene bottle and mixed with distilled water (30 % by mass of the powdered cement paste). The new mixes with a resulting w/b of 0.95 were stored in bottles and rotated slowly along the longitudinal axis for additional 7 days at 20 °C. Each moist cement paste was crushed and homogenized with a stainless steel bar, resulting in a sample with the appearance as “moist sand”. This procedure for preparation of the pastes aims to maximize the degree of hydration of the cement pastes and minimize possible carbonation prior to chloride exposure [37, 41]. Moreover, a possible minor degree of bleeding for the freshly prepared pastes (w/b = 0.50) may only give minor contribution to heterogeneity in the samples as they have been ground and rehydrated with additional water after 2 months of hydration.

2.3 Chloride exposure

The well-hydrated pastes were exposed to the chloride solutions by the following procedure: 30.0 g of the hydrated cement paste (w/b = 0.95) was weighed into a 45 mL plastic centrifuge tube and 15.0 mL of the chloride solution was added. A reference sample exposed to the same amount of distilled water was also prepared. The samples were sealed, stored in the plastic centrifuge tubes at 20 °C for 2 months and shaken regularly prior to analysis. The samples were prepared with different numbers of replicates (one reference sample for distilled water, two samples for the 0.125, 0.25, and 2.0 mol/L chloride-ion solutions, and three samples for the 0.50 and 1.0 mol/L chloride-ion concentrations).

2.4 Methods

2.4.1 Thermodynamic modeling

Thermodynamic modeling was carried out using the Gibbs free energy minimization software GEMS 3.3 [45, 46], which calculates the equilibrium phase assemblages in chemical systems from their total bulk elemental composition. The default databases were expanded with the CEMDATA14 database [45, 46] including solubility products of the solids relevant for cementitious materials. For the C-S-H phase, the CSHQ model proposed by Kulik [47] was used.

The changes in phase assemblages upon exposure to the chloride solutions were predicted for the different blends. The phase compositions of the chloride-free blends after hydration for 91 days (> 70 days of sample preparation) were calculated using the degrees of hydration for alite, belite, and metakaolin, as determined by ^{29}Si MAS NMR [43] (*c.f.*, Table 3). These data indicate that only a minor increase in the degree of hydration takes place during the chloride exposure; full hydration is assumed for the calcium aluminate phase as supported by ^{27}Al MAS NMR [43].

The effect of the NaCl and $CaCl_2$ solutions was modelled for chloride concentrations between 0.0 and 2.0 mol/L, employing the same amount of water as in the experiments (*i.e.*, 192.5 g water per 100 g anhydrous cement blend including the mixing water of the pastes). This allows prediction of the progressive change in phases with increasing chloride concentration after reaching an equilibrium condition. The activity coefficients were calculated using the extended Debye–Hückel equation in the Truesdell–Jones form with ion size and extended term parameter for NaCl ($å$ = 3.72 Å and b_γ = 0.064 kg/mol) [48], which is applicable up to an ionic strength of approx. 1 - 2 mol/L [49]. While at higher ionic strength the use of the Pitzer activity corrections would result in more precise aqueous concentrations, the use of extended Debye–Hückel equation has no significant effect on the amount of solid phases calculated in the system studied. During the calculations, the following simplifications were made:

(i) The uptake of alkali ions by the C-S-H phase is taken into account by employing an ideal solid-solution model between the C-S-H phase and two hypothetical alkali silicate hydrates, $((KOH)_{2.5}SiO_2H_2O)_{0.2}$ and $((NaOH)_{2.5}SiO_2H_2O)_{0.2}$ [50], as proposed by Kulik *et al.* [51].

(ii) The uptake of aluminum and sulfur by the C-S-H is taken into account by using the reported Al/Si [43] and S/Si [52] ratios summarized in Table 2. The release of Al from C_3S and C_2S during hydration is also considered in the calculations.

(iii) The model for Kuzel's salt and Friedel's salt includes pure Kuzel's salt and Friedel's salt and solid solutions of Friedel's salt with carbonate (CO_3_AFm) and hydroxide (OH_AFm) [53].

(iv) The uptake of chloride ions by the C-S-H is not taken into account. It will be estimated by subtracting the chloride content in Friedel's salt from the total bound chloride.

2.4.2 Thermogravimetric analysis

Thermogravimetric analysis (TGA) was performed directly on moist paste samples after two months of chloride exposure. A Mettler Toledo TGA/SDTA 851 instrument was used. About 1.0 g of the sample was loaded in a 900 µL alumina crucible and dried at 40 °C in the TGA chamber purged with N_2 for 4 – 5 h, followed by heating up to 950 °C at rate 10 °C/min. Friedel's salt formed in the pastes can be identified by TGA from the second of the two main dehydroxylation peaks for Friedel's salt in the temperature ranges 100 – 150 °C and 230 – 410 °C after chloride exposure. The two weight-loss regions reflect the release of four water molecules from the interlayer between 100 to 150°C and six water from the main layer of the Friedel's salt structure at 230 – 410 °C [7, 54-56].

2.4.3 X-ray diffraction analysis

The samples used for the X-ray diffraction analysis (XRD) are the same as those used for TGA. However, the hydration of the paste samples was stopped by immersing the sample first in 60 ml of isopropanol for 15 minutes. After filtration the residues were rinsed first with isopropanol and then with diethyl ether. Subsequently, the pastes were dried at 40 °C for 5 minutes and gently ground by hand in an agate mortar. Preparation for the XRD measurements was performed by backloading. The samples were measured without and with 20% CaF_2, which was added as internal standard to quantify the total amount of amorphous and minor crystalline phases. A PANalytical X'Pert Pro MPD diffractometer with Cu$K\alpha_1$ radiation in a θ – 2θ configuration was used. The samples were scanned between 5 – 70° 2θ with the X'Celerator detector during 60 minutes, applying an incident beam monochromator, a 0.5° divergence slit, a 1° anti-scattering slit on the incident beam side and a 0.04 rad Soller slit on the diffracted beam side. Rietveld refinements were performed using X'Pert HighScore Plus V. 3.0.5 using the crystal structures reported in ref. [57]. The background was fitted manually using base points. The refinement procedure included the scale factors, lattice parameters, peak shape parameters and preferred orientation for Friedel's salt.

2.4.4 Determination of the chloride binding isotherms

The "free water" content of the wet pastes (w/b=0.95) has been determined by thermogravimetric analysis (TGA) prior to the chloride exposure. Approximately 1.0 g of the wet paste was dried at 40 °C (and not at 105 °C as used recently [37, 41]) in the TGA chamber purged with N_2 for 4 – 5 h during which the weight of sample stabilized. The measured weight loss at 40 °C ("free water" content) was 30.4 wt.% (P), 29.5 wt.% (ML) and 31.4 wt.% (M) of the initial weight of the corresponding wet pastes. The chloride exposed paste samples stored in the tubes were shaken and subsequently centrifuged after 2 months of chloride exposure. However, it should be kept in mind that centrifuging extraction will not 100% remove the free chloride ions from the pore solution, which will result in slightly higher amount of total bound chloride reported. The pH was measured using a Metrohm 6.0255.100 Profitrode calibrated with buffer solutions at predefined pH of 7.0, 10.0 and 13.0. The chloride concentration of the extracted liquid phase at equilibrium was determined by potentiometric titration with 0.010 M $AgNO_3$(*aq*) using a Titrando 905 from Metrohm. A high-resolution Element 2 ICP-MS from Thermo Scientific was used to determine the concentration of calcium in solution. The solutions analyzed by ICP-MS were acidified to obtain a HNO_3 concentration of 0.10 mol/L.

The chloride binding isotherms were obtained following recently described calculations [41], which are summarized below. The initial chloride concentration ($C_{Cl,initial}$) is calculated from the chloride concentration of the added solution ($C_{Cl,added}$) as follows:

$$C_{Cl,initial} = \frac{C_{Cl,added} \times V_{Cl,added}}{V_{H_2O} + V_{Cl,added}} \quad (1)$$

where $V_{Cl,added}$ is 15.0 mL and V_{H_2O} is the volume of "free water" available in 30.0 g of hydrated paste sample which is 30.0 g × 30.4 wt.% = 9.1 g ≈ 9.1.0 mL for the P sample and 8.9 mL and 9.4 mL for the ML (29.5 wt.% of free water) and M (31.4 wt.% of free water) samples, respectively. The bound chloride content ($C_{Cl,total\ bound}$) is calculated from the measured equilibrium chloride concentration in the liquid phase ($C_{Cl,eq}$) by the relation:

$$C_{Cl,total\ bound} = \frac{M_{Cl} \times (C_{Cl,initial} - C_{Cl,eq}) \times (V_{H2O} + V_{Cl,added})/1000}{m_{sample}/(1+0.95)} \quad (2)$$

with M_{Cl} = 35.45 g/mol, m_{sample} = 30.0 g, 0.95 being the w/b ratio of the wet pastes, and $m_{sample}/(1 + 0.95)$ as the amount of unhydrated cement blend needed for producing 30.0 g of

the resulting paste. Thus, the bound chloride content is reported as g/g of unhydrated cement blend. In the present study, the discussion on the chloride binding is based on the general agreement from published studies that the major phases for binding chloride are Friedel's salt and the C-S-H. The possible minor uptake of chloride ions by other phases (*e.g.* ettringite and portlandite etc.), as reported in the literature [58], and possible physical adsorption of chloride on the positive charged surface of Friedel's salt [58] is considered to be negligible. Thus, the amount of chloride associated with the C-S-H (Cl_{C-S-H}) can be estimated from the measured total bound chloride (Cl_{total}) by subtraction of the chloride content in Friedel's salt (Cl_{Fs}) predicted by thermodynamic modeling, *i.e.*,

$$C_{Cl,C-S-H} = C_{Cl,\text{total bound}} - C_{Cl,Fs} \quad (3)$$

In addition, the calcium binding isotherm reflecting the uptake of calcium by hydration products from the $CaCl_2$ solution has also been determined. The initial calcium concentration is calculated as $C_{Ca,initial} = C_{Cl,initial}/2$ based on the charge balance. The bound calcium ($C_{Ca,bound}$) is calculated from the measured equilibrium calcium concentration ($C_{Ca,eq}$) and the initial calcium concentration ($C_{Ca,initial}$) in the liquid phase according to Eq. (4):

$$C_{Ca,bound} = \frac{M_{Ca} \times (C_{Ca,initial} - C_{Ca,eq}) \times (V_{H2O} + V_{Ca,added})/1000}{m_{sample}/(1+0.95)} \quad (4)$$

where $V_{Ca,added} = V_{Cl,added}$, M_{Ca} = 40.08 g/mol. It should be noted that the Ca^{2+} ions dissolved from hydration products in the pore solution are not taken into account in $C_{Ca,initial}$, but may not be excluded for $C_{Ca,eq}$.

3 Results and discussion

3.1 Phase assemblages

3.1.1 Thermodynamic modeling

Thermodynamic modeling is employed to predict the phase assemblages for the P, ML and M pastes exposed to the NaCl and $CaCl_2$ solutions as shown in Fig. 1. It is predicted that the main hydrates in the P paste before chloride exposure are C-S-H (Ca/Si=1.63), portlandite ($Ca(OH)_2$), ettringite ($Ca_6Al_2(SO_4)_3(OH)_{12}\cdot 26H_2O$), monocarbonate ($Ca_4Al_2CO_3(OH)_{12}\cdot 5H_2O$), calcium carbonate ($CaCO_3$) and a minor amount of hydrotalcite ($Mg_4Al_2(OH)_{14}\cdot 3H_2O$). Similar hydrates are predicted for the ML and M pastes, although the C-S-H phase exhibits a lower

Ca/Si ratio of 1.29 and no portlandite remains as a result of the pozzolanic reaction of metakaolin. In addition, the presence of strätlingite ($Ca_4Al_2(OH)_{12}[AlSi(OH)_8]_2 \cdot 2H_2O$) is predicted for the M paste. The predicted phase assemblages for the P, ML and M pastes are in good agreement with the experimental data obtained by XRD, ^{27}Al and ^{29}Si MAS NMR [43].

When the NaCl and $CaCl_2$ solutions are added to the hydrated P and ML pastes, the replacement of monocarbonate with consumption of calcium from portlandite or the $CaCl_2$ solution by Friedel's salt ($Ca_4Al_2Cl_2(OH)_{12} \cdot 4H_2O$) and calcium carbonate is predicted, according to Eqs. (5) and (6). A slight reduction of the amount of ettringite is also predicted as seen in Fig. 1.

$$Ca_4Al_2CO_3(OH)_{12} \cdot 5H_2O + 2\ NaCl + Ca(OH)_2 \rightarrow Ca_4Al_2Cl_2(OH)_{12} \cdot 4H_2O + CaCO_3 + 2\ Na^+ + 2\ OH^- + H_2O \quad (5)$$

$$Ca_4Al_2CO_3(OH)_{12} \cdot 5H_2O + CaCl_2 \rightarrow Ca_4Al_2Cl_2(OH)_{12} \cdot 4H_2O + CaCO_3 + H_2O \quad (6)$$

For the M paste, a destabilization of some ettringite and the formation of Kuzel's salt ($Ca_4Al_2Cl(SO_4)_{0.5}(OH)_{12} \cdot 6H_2O$) are predicted at low chloride concentration. At higher chloride concentrations, instead Friedel's salt formation is calculated and the destabilization of strätlingite and calcium from high-Ca C-S-H (similar to the destabilization of calcium from portlandite) to Friedel's salt and low-Ca C-S-H is predicted. The conceptual reaction is exemplified in Eq. (7), where the high-Ca C-S-H is represented by $Ca(OH)_2$ on the reactant side whereas $CaO \cdot SiO_2 \cdot 2H_2O$ corresponds to a low-Ca C-S-H phase on the product side. Thus, Eq. (7) shows that the destabilization of strätlingite is associated with a reduction of the Ca/Si ratio in the C-S-H. The amount of Friedel's salt formed in the ML and M pastes in the presence of NaCl is limited by the availability of calcium and thus also a very small amount or no precipitation of calcium carbonate is calculated. Transformation of monocarbonate to Friedel's salt with precipitation of calcium carbonate is predicted for the M paste only when it is exposed to the $CaCl_2$ solution.

$$Ca_2Al_2SiO_4(OH)_6 \cdot 5H_2O + 2\ NaCl + 3\ Ca(OH)_2 + 2\ H_2O \rightarrow Ca_4Al_2Cl_2(OH)_{12} \cdot 4H_2O + 2\ Na^+ + 2\ OH^- + CaO \cdot SiO_2 \cdot 2H_2O \quad (7)$$

3.1.2 Thermogravimetric analysis

The presence of Friedel's salt in the P, ML and M pastes after exposure to the NaCl and $CaCl_2$ solutions is analyzed by TGA, and the differential thermogravimetric (DTG) curves are shown in Fig. 2. The DTG curves for the P paste exposed to distilled water show the presence of C-S-H, ettringite and monocarbonate (50 – 300 °C), portlandite (400 – 600 °C) and calcium carbonate (600 – 800 °C). For the ML and M pastes exposed to distilled water, minor amounts of portlandite are still detected as a result of the heterogeneity of the hydrating material. Furthermore, decomposition of strätlingite at about 250 °C is observed for the M paste. The results are generally in good agreement with those observed for mortars made from the same binder materials [7, 24, 26] and with the phase assemblages predicted by thermodynamic modeling in Fig. 1.

For all pastes exposed to the NaCl and $CaCl_2$ solutions at high chloride concentration, additional weight losses (150 – 200 °C and 280 – 400 °C) related to Friedel's salt are observed, as shown in Fig. 2. The results show that the intensity of the DTG peaks associated with the six main layer water molecules in Friedel's salt (280 – 400 °C) increases with increasing chloride concentration. The formation of Friedel's salt at higher concentrations is accompanied by a consumption of the monocarbonate and/or strätlingite phases as observed from the weight loss at lower temperature around 200 – 250 °C in the DTG curves. Clearly, more Friedel's salt is observed in the metakaolin containing blends, in particular in the presence of high $CaCl_2$ concentrations. The identification and transformation of phases observed by TGA confirm the results predicted by thermodynamic modeling (Fig. 1).

3.1.3 X-ray diffraction analysis

The changes in phase assemblages for the P, ML and M pastes exposed to different chloride concentrations of the $CaCl_2$ solution are also analyzed by XRD as shown in Fig. 3. The XRD patterns show that the main crystalline hydration products detected in the P paste are ettringite and portlandite. For the ML and M pastes, minor amounts of portlandite are detected, whereas large amounts of monocarbonate and strätlingite are observed in the ML and M pastes, respectively. With increasing chloride concentration from 0.25 mol/L to 1.0 mol/L and 2.0 mol/L, the intensity of the reflections associated with Friedel's salt increases followed by the decrease of the reflection intensity for monocarbonate and strätlingite. A minor reflection associated with Kuzel's salt is also detected for the M paste exposed 0.25 mol/L $CaCl_2$ solution. The results observed from the XRD patterns confirm those observed from the DTG curves (Fig. 2) and those predicted by thermodynamic modeling (Fig. 1).

3.2 Total chloride binding isotherms

3.2.1 Effect of the types of cations and binder composition

The total chloride binding isotherms for the P, ML and M pastes exposed to the NaCl and $CaCl_2$ solutions of varying chloride concentrations are given in Fig. 4. The isotherms are calculated following the methods described in *section 2.4.4* by using the measured concentrations presented in Table 4. A higher total chloride binding is observed not only for the P paste but also for the ML and M pastes when they are exposed to the $CaCl_2$ solution as compared to the corresponding paste exposed to the NaCl solution. Similar observations for chloride-exposed hydrated Portland cement can also be found in several other studies [17, 32, 35-37]. This observation implies that calcium in the exposure solution plays an important role in enhancing chloride binding for both hydrated Portland cement and blended cements. The role of calcium on chloride binding will be further discussed in *section 3.5*.

The results in Fig. 4 also show that partial substitution of the wPc with MK or MK and LS increases the total chloride binding. This observation is consistent with earlier studies [13, 59] and with the higher amount of Friedel's salt in the blended cement systems predicted by thermodynamic modeling (Fig. 1). There is no major difference in total chloride binding between the ML and M pastes.

3.3 Assessment of the chloride distribution in solids

3.3.1 Chloride bound as Friedel's salt

The present work utilizes the results of the degree of reaction for the principal phases from a ^{29}Si NMR study of paste samples of the same blends by Dai [43] in combination with thermodynamic modeling to quantify the amount of Friedel's salt formed. The results are compared with those from XRD/Rietveld analysis performed on several selected samples as shown in Fig. 5a. The good agreement between the thermodynamic calculations and XRD/Rietveld analysis suggests a reliable prediction of the Friedel's salt content from thermodynamic modeling. The calculated amounts of Cl bound as Friedel's salt by thermodynamic modeling is presented in Fig. 5b. For the P pastes, the results show that the constant (maximum) amount of chloride binding by the formation of Friedel's salt is independent on the type of cations. Based on the obtained amount of Friedel's salt together with the calcium aluminate (C_3A) content of the studied Portland cement, it can be calculated that only 20 % of the C_3A is consumed for the formation of the actual amounts of Friedel's salt,

418 which is consistent with the fraction determined for chloride exposed mortars in a parallel
419 study [7]. The main fraction of aluminum remains in the ettringite phase as predicted by
420 thermodynamic modeling. For the ML and M pastes, thermodynamic modeling shows that the
421 maximum binding capacity with respect to transformation of the maximum amount of
422 monocarbonate has not been obtained for the ML and M pastes exposed to the NaCl solution
423 (Fig. 1c,e). This is related to the limited availability of calcium, which prevents the further
424 formation of Friedel's salt as exemplified in Eq. (7). Similar to the present study, an earlier
425 study of ten hydrated cement pastes containing limestone and different pozzolanic materials
426 [60] reported that the presence of alkalis hinders the formation of chloride-bearing AFm phases.
427 According to the present work, this can be explained by an insufficient amount of calcium in
428 the exposure solution, inhibiting the transformation of strätlingite and/or monocarbonate to
429 Friedel's salt according to Eqs. (5), (6) and (7). For all samples, thermodynamic modeling also
430 predicts that the formation of Friedel's salt starts at lower chloride concentration for the $CaCl_2$
431 exposure as compared to the NaCl exposure, (e.g. 0.2 mol/L vs. 0.4 mol/L for ML pastes). This
432 finding indicates that calcium plays an important role in facilitating the formation of Friedel's
433 salt.
434 Several studies have reported that the addition of alumina-rich SCMs increase the chloride
435 binding due to formation of an additional amount of Friedel's salt. This is confirmed in the
436 present study by thermodynamic modeling and the amounts of Friedel's salt obtained from
437 XRD/Rietveld analysis in Fig. 5. Both the experimental and thermodynamic modeling data
438 show that a higher amount of Friedel's salt is formed for the metakaolin blends as compared to
439 the plain Portland cement.
440
441 **3.3.2 Chloride associated with C-S-H**
442 An attempt to evaluate the relative differences in chloride content associated with the C-S-H
443 phase is made for the samples exposed to chloride solutions with different associated cations
444 (*i.e.*, Na^+ and Ca^{2+}). No significant chloride binding in the C-S-H phase is observed for the M
445 and ML pastes as seen by comparing the data from Fig. 4b and Fig. 5b. The chloride ions
446 associated with the C-S-H in the P samples are shown in Fig. 6. These data are obtained by
447 subtracting the chloride bound as Friedel's salt obtained from thermodynamic modelling from
448 the amount of total bound chloride. For the P sample (Fig.6a), it is clear that the presence of an
449 additional amount of Ca^{2+} ions in the exposure solution increases the amount of chloride in the
450 diffuse layer of the C-S-H phase as compared to the NaCl solution. According to the studies of
451 Nonat and coworkers [28, 61], this can be explained by the sorption of calcium onto the

negatively charged C-S-H surface, according to Eq. (8), which can lead to a positively charged surface at higher calcium concentrations. In the presence of chloride, this positively charged surface is compensated by chloride ions in the diffuse layer of the C-S-H phase according to Eq. (9) as described in earlier studies [28, 30].

$$\equiv SiO^- + Ca^{2+} \leftrightarrow \equiv SiO^-Ca^{2+} \quad (8)$$

$$\equiv SiO^-Ca^{2+} + 2Cl^- \leftrightarrow \equiv SiO^-Ca^{2+}2Cl^- \quad (9)$$

3.3.3 Contribution from Friedel's salt and the C-S-H phase to the total chloride binding

Based on the discussion above, the contribution from Friedel's salt and the C-S-H phase to the total chloride binding can potentially be evaluated. For the P paste exposed to the NaCl solution, the total chloride binding and its maximum binding capacity (Fig. 4a) are mainly determined by the chloride binding as Friedel's salt. When the P paste is exposed to the $CaCl_2$ solution, the higher and continuous increase in the total chloride binding (Fig. 4b) originates from chloride in the diffuse layer of the C-S-H (Fig. 6a), since the maximum chloride binding as Friedel's salt is reached (Fig. 5b). An increase in the total chloride binding is observed when metakaolin is used to replace Portland cement (Fig. 4a, b), which is ascribed to the formation of more Friedel's salt rather than chloride binding in the C-S-H phase, since there is no clear evidence of a chloride adsorption on the C-S-H phase in the ML and M pastes.

3.4 pH values

3.4.1 Effect of the exposure solution on pH

The measured pH values for the supernatants of the NaCl and $CaCl_2$ exposure solutions for the P, ML and M pastes are shown in Table 4 and Fig. 7. The results show a lower pH for the ML and M pastes than for the P paste as already observed for hydrated blended cements [62]. There is a minor increase in pH when the pastes are exposed to NaCl solutions compared to the pastes exposed to distilled water, which has also been observed earlier [37]. The increased pH in the presence of NaCl(*aq*) is assumed to be related to the conversion of monocarbonate and portlandite to Friedel's salt, calcium carbonate and sodium hydroxide as described by Eq. (5), which results in an increase of the OH^-(*aq*) concentration. A significant decrease in pH is observed with increasing chloride concentrations when the pastes are exposed to the $CaCl_2$ solutions as also reported in other studies [36, 37, 63]. The decrease in pH upon the presence of $CaCl_2$(*aq*) is not related to the conversion of monocarbonate to Friedel's salt (see Eq. (6)), but it may be caused by a calcium uptake by the C-S-H phase, since at high calcium concentrations,

Ca^{2+} can be adsorbed on the surface of the C-S-H [30, 61, 64], leading to a release of charge balancing H^+ ions from the silanol groups to the exposure solution according to Eq. (8).

3.4.2 Relationship between pH and chloride binding

The relationship between the total amount of bound chloride and the pH of the exposure solutions for P, ML and M pastes exposed to the NaCl and $CaCl_2$ solutions are shown in Fig. 8. Since the changes in pH for the NaCl exposure solutions are small, only a minor effect of pH on the binding is observed and the increased chloride binding for the pastes exposed to NaCl solutions is mainly driven by the formation of Friedel's salt. In contrast, an apparent correlation between the total bound chloride and pH is obtained for the P paste exposed to the $CaCl_2$ solution (Fig. 8a) as reported recently [37]. For the P paste, a small fraction of chloride can be bound in Friedel's salt as the studied Portland cement only forms a small amount of AFm phases upon hydration. The additional uptake observed in the presence of $CaCl_2$(*aq*) but not in the case of NaCl(*aq*) is thus related to chloride ions present in the diffuse layer of C-S-H. A similar increase of chloride binding with decreasing pH has also been reported in earlier studies [36, 37, 63]. The increased total chloride binding with lower pH has been ascribed to less competition with OH^- ions and thus a larger Cl^- uptake by the C-S-H [36, 38]. A similar correlation can also be observed for the blended cements containing metakaolin with or without limestone exposed to the $CaCl_2$ solution (Fig. 8b). Different from the P paste, the additional uptake of chloride observed for the M and ML pastes in the presence of the $CaCl_2$ solution compared to the NaCl solution is related to chloride ions present in Friedel's salt and not in the diffuse layer of the C-S-H (Fig. 5b).

3.5 Role of calcium in chloride binding

3.5.1 Relationship between pH and the calcium concentration

The impact of cations on chloride binding is related to the availability of calcium as discussed above for Friedel's salt and as observed by the amount of chloride ions in the diffuse layer of the C-S-H in published studies [28, 30]. The apparent pH dependency of the chloride binding in the case of $CaCl_2$ exposure (Fig. 8) can be explained by the intrinsic relation between pH and the calcium concentrations of the pore solution as shown in Fig. 9, which is constructed using the data in Table 4. The results show that the pH decreases with increased $CaCl_2$ concentration for the exposure solution for all the studied cement pastes. For this reason, the uptake of calcium from the $CaCl_2$ exposure solution and its effect on the amount of total bound chloride and chloride associated with the C-S-H will be evaluated in more detail below.

3.5.2 Total calcium binding from the $CaCl_2$ solution

Similar to chloride binding, also the calcium ions added are taken up by cement hydrates in the P, ML and M pastes as shown in Fig. 10. The uptake of calcium by the cement pastes increases with increasing $CaCl_2$ concentration in the exposure solution, as expected. This trend is found to be similar to that of the total chloride binding isotherm (Fig. 4). The increment of both the calcium and chloride binding decreases at high chloride concentration, indicating that a maximum calcium and chloride binding capacity is present in the hydrated cement blends. In addition, both the calcium and chloride binding are found to be higher for the ML and M pastes than for the P paste as expected, since a larger amount of calcium ions are needed to accommodate the released carbonate from monocarbonate for the formation of Friedel's salt.

3.5.3 Relationship between bound chloride and bound calcium

The relationship between total bound chloride and total "bound" calcium (*i.e.*, uptake of calcium from the $CaCl_2$ exposure solution by hydration products) for the studied pastes is shown in Fig. 11. The data show a linear correlation between the amount of total bound chloride and the total "bound" calcium content from the $CaCl_2$ solution. More interestingly, the ratio between total bound chloride and calcium is close to Cl/Ca = 2, independent of the type of studied cement blend. The linear correlation between the bound Ca and bound chloride is ascribed to the following mechanisms: (*i*) calcium promotes the formation of Friedel's salt (uptake of two chloride ions) plus $CaCO_3$ (one calcium) from monocarbonate according to Eq. (6) and (*ii*) calcium increases the amount of chloride in the diffuse layer of the C-S-H, as shown by Eq. (9) and discussed in a recent study [30]. Overall, the results confirm that the amount of bound calcium has a closer relation with the chloride binding than effects from pH. No relationship between the bound chloride and bound calcium can be obtained for the P, ML and M pastes exposed to the NaCl solutions, which reflects that no additional calcium is introduced into these systems.

4 Conclusions

The chloride binding of Portland cement (P) – metakaolin (M) – limestone (L) blends exposed to different concentrations of NaCl and $CaCl_2$ solutions has been investigated and based on the analysis of the results from TGA, XRD, exposure solution elemental analysis and thermodynamic modeling, the following conclusions can be drawn:

(1) The use of metakaolin in Portland cement blends increases the chloride-binding capacity compared to pure Portland cement. This is attributed to the formation of a larger quantity of Friedel's salt in the ML and M samples as compared to the P samples and it reflects that metakaolin acts as an additional aluminum source.

(2) A larger quantity of chloride is bound in the P samples exposed to the $CaCl_2$ solution as compared to the NaCl solution. This is ascribed to the higher amount of available calcium ions, which enhances the presence of chloride ions in the diffuse layer of the C-S-H, whereas the amount of Friedel's salt is independent of the type of cation in the NaCl or $CaCl_2$ exposure solutions. For the ML and M samples exposed to the $CaCl_2$ solution, the increased chloride binding, as compared to NaCl exposure solution, is ascribed to the higher calcium concentrations, which increase the formation of Friedel's salt. A schematic drawing summarizing the distribution of chloride ions in the hydrated cement blends is shown in Fig. 12.

(3) The pH is found to decrease with increasing $CaCl_2$ concentration as a result of the calcium binding on the C-S-H surface resulting in a release of protons, whereas a minor increase in pH is observed for increasing NaCl concentration as a result of the conversion of monocarbonate to Friedel's salt and calcium carbonate.

(4) Independent of the type of cement blends, the present results indicate that the calcium concentration has a decisive role for the chloride binding as the uptake of chloride is found to be coupled with the consumption of calcium from the exposure solution. A linear correlation between the amounts of total bound chloride and total "bound" calcium from the $CaCl_2$ exposure solution has been established with a Cl/Ca ratio close to 2:1.

Acknowledgements

The Danish Council for Strategic Research is acknowledged for financial support to the LowE-CEM project (No. 11-116724).

578 **References**

579 [1] L. Bertolini, B. Elsener, P. Pedeferri, E. Redaelli, R.B. Polder, Corrosion of steel in
580 concrete: prevention, diagnosis, repair, John Wiley & Sons, 2013.
581 [2] Q. Yuan, C. Shi, G. De Schutter, K. Audenaert, D. Deng, Chloride binding of cement-
582 based materials subjected to external chloride environment–a review, Construction and
583 Building Materials, 23 (2009) 1-13.
584 [3] U. Angst, B. Elsener, C.K. Larsen, Ø. Vennesland, Critical chloride content in reinforced
585 concrete—a review, Cement and Concrete Research, 39 (2009) 1122-1138.
586 [4] X. Shi, N. Xie, K. Fortune, J. Gong, Durability of steel reinforced concrete in chloride
587 environments: An overview, Construction and Building Materials, 30 (2012) 125-138.
588 [5] I. Galan, F.P. Glasser, Chloride in cement, Advances in Cement Research, 27 (2015) 63-
589 97.
590 [6] R. Loser, B. Lothenbach, A. Leemann, M. Tuchschmid, Chloride resistance of concrete
591 and its binding capacity–Comparison between experimental results and thermodynamic
592 modeling, Cement and Concrete Composites, 32 (2010) 34-42.
593 [7] Z. Shi, M.R. Geiker, B. Lothenbach, K. De Weerdt, S. Ferreiro Garzón, K. Enemark-
594 Rasmussen, J. Skibsted, Friedel's salt profiles from thermogravimetric analysis and
595 thermodynamic modelling of Portland cement-based mortars exposed to sodium
596 chloride solution, Cement and Concrete Composites, (in press 2017).
597 [8] V. Baroghel-Bouny, X. Wang, M. Thiery, M. Saillio, F. Barberon, Prediction of chloride
598 binding isotherms of cementitious materials by analytical model or numerical inverse
599 analysis, Cement and Concrete Research, 42 (2012) 1207-1224.
600 [9] D.P. Bentz, E.J. Garboczi, Y. Lu, N. Martys, A.R. Sakulich, W.J. Weiss, Modeling of the
601 influence of transverse cracking on chloride penetration into concrete, Cement and
602 Concrete Composites, 38 (2013) 65-74.
603 [10] G.K. Glass, N.R. Buenfeld, The influence of chloride binding on the chloride induced
604 corrosion risk in reinforced concrete, Corrosion Science, 42 (2000) 329-344.
605 [11] B. Martın-Pérez, H. Zibara, R. Hooton, M. Thomas, A study of the effect of chloride
606 binding on service life predictions, Cement and Concrete Research, 30 (2000) 1215-
607 1223.
608 [12] E. L'Hôpital, N. Seigneur, M. Voutilainen, A. Dauzères, Transport properties of cement
609 model system (C3S and C-S-H): Experiments dedicated to implement a new approach
610 of the microstructure / diffusion properties relation in the reactive transport code, in:

611 4th International Workshop on Mechanisms and Modelling of Waste / Cement
612 Interactions May 22-25, 2016, Murten, Switzerland, 2016.
613 [13] M. Thomas, R. Hooton, A. Scott, H. Zibara, The effect of supplementary cementitious
614 materials on chloride binding in hardened cement paste, Cement and Concrete
615 Research, 42 (2012) 1-7.
616 [14] R. Dhir, M. El-Mohr, T. Dyer, Chloride binding in GGBS concrete, Cement and Concrete
617 Research, 26 (1996) 1767-1773.
618 [15] R. Luo, Y. Cai, C. Wang, X. Huang, Study of chloride binding and diffusion in GGBS
619 concrete, Cement and Concrete Research, 33 (2003) 1-7.
620 [16] R.K. Dhir, M.A.K. El-Mohr, T.D. Dyer, Developing chloride resisting concrete using
621 PFA, Cement and Concrete Research, 27 (1997) 1633-1639.
622 [17] C. Arya, N. Buenfeld, J. Newman, Factors influencing chloride-binding in concrete,
623 Cement and Concrete Research, 20 (1990) 291-300.
624 [18] C. Arya, Y. Xu, Effect of cement type on chloride binding and corrosion of steel in
625 concrete, Cement and Concrete Research, 25 (1995) 893-902.
626 [19] C.S. Poon, S.C. Kou, L. Lam, Compressive strength, chloride diffusivity and pore
627 structure of high performance metakaolin and silica fume concrete, Construction and
628 Building Materials, 20 (2006) 858-865.
629 [20] S. Wild, J. Khatib, A. Jones, Relative strength, pozzolanic activity and cement hydration
630 in superplasticised metakaolin concrete, Cement and Concrete Research, 26 (1996)
631 1537-1544.
632 [21] K. De Weerdt, K. Kjellsen, E. Sellevold, H. Justnes, Synergy between fly ash and
633 limestone powder in ternary cements, Cement and Concrete Composites, 33 (2011) 30-
634 38.
635 [22] K. De Weerdt, H. Justnes, K.O. Kjellsen, E. Sellevold, Fly ash-limestone ternary
636 composite cements: synergetic effect at 28 days, Nordic Concrete Research, 42 (2010)
637 51-70.
638 [23] M. Steenberg, D. Herfort, S. Poulsen, J. Skibsted, J. Damtoft, Composite cement based on
639 Portland cement clinker, limestone and calcined clay, in: 13th International Congress
640 of the Chemistry of Cement, Madrid, 2011, pp. 97.
641 [24] M. Antoni, J. Rossen, F. Martirena, K. Scrivener, Cement substitution by a combination
642 of metakaolin and limestone, Cement and Concrete Research, 42 (2012) 1579-1589.

[25] K. Scrivener, A. Favier, (Eds.). Calcined Clays for Sustainable Concrete: Proceedings of the 1st International Conference on Calcined Clays for Sustainable Concrete, Springer, 2015.

[26] Z. Shi, B. Lothenbach, M.R. Geiker, J. Kaufmann, A. Leemann, S. Ferreiro, J. Skibsted, Experimental studies and thermodynamic modeling of the carbonation of Portland cement, metakaolin and limestone mortars, Cement and Concrete Research, 88 (2016) 60-72.

[27] Z. Shi, M.R. Geiker, K. De Weerdt, B. Lothenbach, J. Kaufmann, W. Kunther, S. Ferreiro, D. Herfort, J. Skibsted, Durability of Portland cement blends including calcined clay and limestone: interactions with sulfate, chloride and carbonate ions, in: Calcined Clays for Sustainable Concrete, Springer, 2015, pp. 133-141.

[28] G. Plusquellec, A. Nonat, Interactions between calcium silicate hydrate (C-S-H) and calcium chloride, bromide and nitrate, Cement and Concrete Research, 90 (2016) 89-96.

[29] J.J. Beaudoin, V.S. Ramachandran, R.F. Feldman, Interaction of chloride and CSH, Cement and Concrete Research, 20 (1990) 875-883.

[30] G. Plusquellec, A. Nonat, I. Pochard, Anion uptake by calcium silicate hydrate. 32nd Cement and Concrete Science Conference. Belfast. 17 - 18 Sept. 2012 (paper PRE-4), (2012).

[31] V.S. Ramachandran, Possible states of chloride in the hydration of tricalcium silicate in the presence of calcium chloride, Matériaux et Construction, 4 (1971) 3-12.

[32] O. Wowra, M.J. Setzer, Sorption of chlorides on hydrated cement and C3S pastes, in: M.J. Setzer, R. Auberg (Eds.) "Frost Resistance of Concrete" Proceedings of the International RILEM Workshop on Resistance of Concrete to Freezing and Thawing With or Without De-icing Chemicals E & FN Spon, London SE1 8HN, UK, 1997, pp. 155-162.

[33] L. Tang, L.-O. Nilsson, Chloride binding capacity and binding isotherms of OPC pastes and mortars, Cement and Concrete Research, 23 (1993) 247-253.

[34] H. Zibara, R. Hooton, M. Thomas, K. Stanish, Influence of the C/S and C/A ratios of hydration products on the chloride ion binding capacity of lime-SF and lime-MK mixtures, Cement and Concrete Research, 38 (2008) 422-426.

[35] A. Delagrave, J. Marchand, J.-P. Ollivier, S. Julien, K. Hazrati, Chloride binding capacity of various hydrated cement paste systems, Advanced Cement Based Materials, 6 (1997) 28-35.

677 [36] J. Tritthart, Chloride binding in cement II. The influence of the hydroxide concentration
678 in the pore solution of hardened cement paste on chloride binding, Cement and
679 Concrete Research, 19 (1989) 683-691.
680 [37] K. De Weerdt, A. Colombo, L. Coppola, H. Justnes, M. Geiker, Impact of the associated
681 cation on chloride binding of Portland cement paste, Cement and Concrete Research,
682 68 (2015) 196-202.
683 [38] A. Suryavanshi, J. Scantlebury, S. Lyon, Mechanism of Friedel's salt formation in
684 cements rich in tri-calcium aluminate, Cement and Concrete Research, 26 (1996) 717-
685 727.
686 [39] F. Pruckner, O. Gjørv, Effect of $CaCl_2$ and NaCl additions on concrete corrosivity,
687 Cement and Concrete Research, 34 (2004) 1209-1217.
688 [40] Q. Zhu, L. Jiang, Y. Chen, J. Xu, L. Mo, Effect of chloride salt type on chloride binding
689 behavior of concrete, Construction and Building Materials, 37 (2012) 512-517.
690 [41] K. De Weerdt, D. Orsáková, M. Geiker, The impact of sulphate and magnesium on
691 chloride binding in Portland cement paste, Cement and Concrete Research, 65 (2014)
692 30-40.
693 [42] S.L. Poulsen, V. Kocaba, G. Le Saoût, H.J. Jakobsen, K.L. Scrivener, J. Skibsted,
694 Improved quantification of alite and belite in anhydrous Portland cements by 29Si
695 MAS NMR: Effects of paramagnetic ions, Solid State Nuclear Magnetic Resonance, 36
696 (2009) 32-44.
697 [43] Z. Dai, Solid-state ^{27}Al and ^{29}Si MAS NMR investigations of white Portland cement -
698 metakaolin blends (PhD thesis), Aarhus University, in, 2015.
699 [44] K.O. Kjellsen, R.J. Detwiler, O.E. Gjørv, Development of microstructures in plain
700 cement pastes hydrated at different temperatures, Cement and Concrete Research, 21
701 (1991) 179-189.
702 [45] T. Wagner, D.A. Kulik, F.F. Hingerl, S.V. Dmytrieva, GEM-Selektor geochemical
703 modeling package: TSolMod library and data interface for multicomponent phase
704 models, The Canadian Mineralogist, 50 (2012) 1173-1195.
705 [46] D.A. Kulik, T. Wagner, S.V. Dmytrieva, G. Kosakowski, F.F. Hingerl, K.V. Chudnenko,
706 U.R. Berner, GEM-Selektor geochemical modeling package: revised algorithm and
707 GEMS3K numerical kernel for coupled simulation codes, Computational Geosciences,
708 17 (2013) 1-24.
709 [47] D.A. Kulik, Improving the structural consistency of CSH solid solution thermodynamic
710 models, Cement and Concrete Research, 41 (2011) 477-495.

711 [48] H.C. Helgeson, D.H. Kirkham, G.C. Flowers, Theoretical prediction of the
712 thermodynamic behavior of aqueous electrolytes by high pressures and temperatures;
713 IV, Calculation of activity coefficients, osmotic coefficients, and apparent molal and
714 standard and relative partial molal properties to 600 degrees C and 5kb, American
715 Journal of Science, 281 (1981) 1249-1516.
716 [49] B.J. Merkel, B. Planer-Friedrich, D. Nordstrom, Groundwater geochemistry, Springer-
717 Verlag Berlin Heidelberg, 2005.
718 [50] B. Lothenbach, G. Le Saout, M.B. Haha, R. Figi, E. Wieland, Hydration of a low-alkali
719 CEM III/B–SiO2 cement (LAC), Cement and Concrete Research, 42 (2012) 410-423.
720 [51] D. Kulik, J. Tits, E. Wieland, Aqueous-solid solution model of strontium uptake in CSH
721 phases, Geochimica et Cosmochimica Acta, 71 (2007) A530.
722 [52] R. Barbarulo, Comportement des matériaux cimentaires: actions des sulfates et de la
723 température (Ph.D. thesis), in, Université Laval Québec, 2002.
724 [53] M. Balonis, B. Lothenbach, G. Le Saout, F.P. Glasser, Impact of chloride on the
725 mineralogy of hydrated Portland cement systems, Cement and Concrete Research, 40
726 (2010) 1009-1022.
727 [54] U. Birnin-Yauri, F. Glasser, Friedel's salt, $Ca_2Al(OH)_6(Cl,OH)\cdot 2H_2O$: its solid solutions
728 and their role in chloride binding, Cement and Concrete Research, 28 (1998) 1713-
729 1723.
730 [55] R.O. Grishchenko, A.L. Emelina, P.Y. Makarov, Thermodynamic properties and thermal
731 behavior of Friedel's salt, Thermochimica Acta, 570 (2013) 74-79.
732 [56] B. Lothenbach, P. Durdziński, K. De Weerdt, Thermogravimetric analysis, in: K.
733 Scrivener , R. Snellings, B. Lothenbach (Eds.) A Practical Guide to Microstructural
734 Analysis of Cementitious Materials, CRC Press, 2016, pp. 177.
735 [57] R. Snellings, X-ray powder diffraction applied to cement, in: K. Scrivener , R. Snellings,
736 B. Lothenbach (Eds.) A Practical Guide to Microstructural Analysis of Cementitious
737 Materials, CRC Press, 2016, pp. 107-176.
738 [58] Y. Elakneswaran, T. Nawa, K. Kurumisawa, Electrokinetic potential of hydrated cement
739 in relation to adsorption of chlorides, Cement and Concrete Research, 39 (2009) 340-
740 344.
741 [59] N.J. Coleman, C.L. Page, Aspects of the pore solution chemistry of hydrated cement
742 pastes containing metakaolin, Cement and Concrete Research, 27 (1997) 147-154.

743 [60] A. Ipavec, T. Vuk, R. Gabrovšek, V. Kaučič, Chloride binding into hydrated blended
744 cements: The influence of limestone and alkalinity, Cement and Concrete Research, 48
745 (2013) 74-85.
746 [61] C. Labbez, I. Pochard, B. Jönsson, A. Nonat, CSH/solution interface: Experimental and
747 Monte Carlo studies, Cement and Concrete Research, 41 (2011) 161-168.
748 [62] B. Lothenbach, K. Scrivener, R.D. Hooton, Supplementary cementitious materials,
749 Cement and Concrete Research, 41 (2011) 1244-1256.
750 [63] H. Zibara, Binding of external chlorides by cement pastes. (PhD thesis), University of
751 Toronto, Canada., (2001).
752 [64] B. Lothenbach, A. Nonat, Calcium silicate hydrates: Solid and liquid phase composition,
753 Cement and Concrete Research, 78 (2015) 57-70.
754
755

Table 1

Chemical compositions (wt.%), density and Blaine fineness for the starting materials.

	wPc	LS	MK
SiO_2	21.81	3.92	52.84
Al_2O_3	3.56	0.33	39.49
Fe_2O_3	0.24	0.14	1.42
CaO	66.13	53.73	0.22
MgO	1.10	0.35	0.48
K_2O	0.43	0.05	1.00
Na_2O	0.04	0.08	0.05
SO_3	3.37	0.05	0.06
TiO_2	0.21	0.02	0.88
P_2O_5	0.04	0.10	0.11
LOI	2.57	41.8	3.55
Density (kg/m^3)	3080	2700	2530
Blaine fineness (m^2/kg)	387	1211	1891
Carbon content	0.37	-	-
$CaCO_3$	3.1	93.8	-

Table 2

Binder compositions for the produced mortars (wt.%).

Blend	wPc[a]	MK	LS[a]	Al/Si [b]	S/Si [c]
				C-S-H (mol/mol)	
P	100	0	0	0.067	0.03
ML	68.1	25.5	6.4	0.092	0.015
M	68.1	31.9	0	0.1	0.015

[(a)] The wPc contains 3.1 wt.% limestone. Thus, the Portland clinker replacement level is 35.0 wt% for the ML and M blends.

[(b)] Al/Si ratios determined from ^{29}Si MAS NMR for paste samples of the same blends [43].

[(c)] S/Si ratios determined for synthetic C-S-H samples with different Ca/Si ratios [52]. The data are related to the individual samples using the Ca/Si ratios determined for the C-S-H phases in the paste samples in ref. [43].

Table 3

Degrees of hydration (H, %)[a] for alite, belite and MK in hydrated paste samples after 28 – 182 days of hydration in demineralized water [43].

Blend	Alite		belite		MK	
	28d	180d	28d	180d	28d	180d
P	81	95	25	63		
ML	83	86	34	36	48	54
M	86	86	34	34	38	50

[a] Determined from ^{29}Si MAS NMR [43] as $H = (1 - I(t)/I(t=0))$, where $I(t=0)$ and $I(t)$ are the intensities of the individual phases before and after hydration for the time (t), respectively.

Table 4

Measured chloride and calcium concentrations and pH values of the exposure solutions at equilibrium.

Blend	$C_{Cl.added}$ [M]	Replicates[a]	NaCl					$CaCl_2$				
			$C_{Cl.eq}$ [M]	Errors [M]	$C_{Ca.eq}$ [mM]	Errors [mM]	pH	$C_{Cl.eq}$ [M]	Errors [M]	$C_{Ca,eq}$ [mM]	Errors [mM]	pH
P	0	1	0.001	-	10.2	-	12.9	-	-	-	-	12.9
	0.125	2	0.031	0.001	11.9	2.4	13.0	0.019	0.002	15.8	1.7	12.8
	0.25	2	0.081	0.001	8.2	0.34	13.1	0.047	0.000	23.5	1.7	12.8
	0.50	3	0.213	0.008	7.1	0.43	13.1	0.114	0.004	49.1	1.1	12.6
	1.0	3	0.476	0.013	7.3	0.36	13.1	0.285	0.004	126	1.7	12.4
	2.0	2	1.078	0.017	7.5	0.03	13.0	0.695	0.006	349	6.5	12.1
ML	0	1	-	-	-	-	12.4	-	-	-	-	12.4
	0.125	2	0.012	0.001	1.6	0.76	12.6	0.005	0.001	5.5	3.6	12.4
	0.25	2	0.036	0.000	1.2	0.22	12.7	0.012	0.000	3.2	0.3	12.3
	0.50	3	0.137	0.002	1.0	0.11	12.6	0.042	0.001	10.1	0.6	12.1
	1.0	3	0.359	0.002	1.6	0.25	12.6	0.123	0.003	50.4	3.8	11.8
	2.0	2	0.862	0.027	1.6	0.04	12.6	0.491	0.011	227	0.3	11.4
M	0	1	0.001	-	2.8	-	12.4	-	-	-	-	12.4
	0.125	2	0.012	0.000	1.4	0.19	12.6	0.005	0.000	4.6	-	12.3
	0.25	2	0.047	0.001	1.3	0.17	12.6	0.017	0.001	5.0	0.1	12.2
	0.50	3	0.152	0.007	1. 6	0.5	12.6	0.045	0.001	10.8	1.9	12.0
	1.0	3	0.369	0.009	3.8	2.8	12.5	0.122	0.003	56.4	4.4	11.3
	2.0	2	0.892	0.001	2.0	0.14	12.4	0.419	0.013	223	-	10.8

[a] The measured chloride and calcium concentrations are the average of the values for the number of replicates.

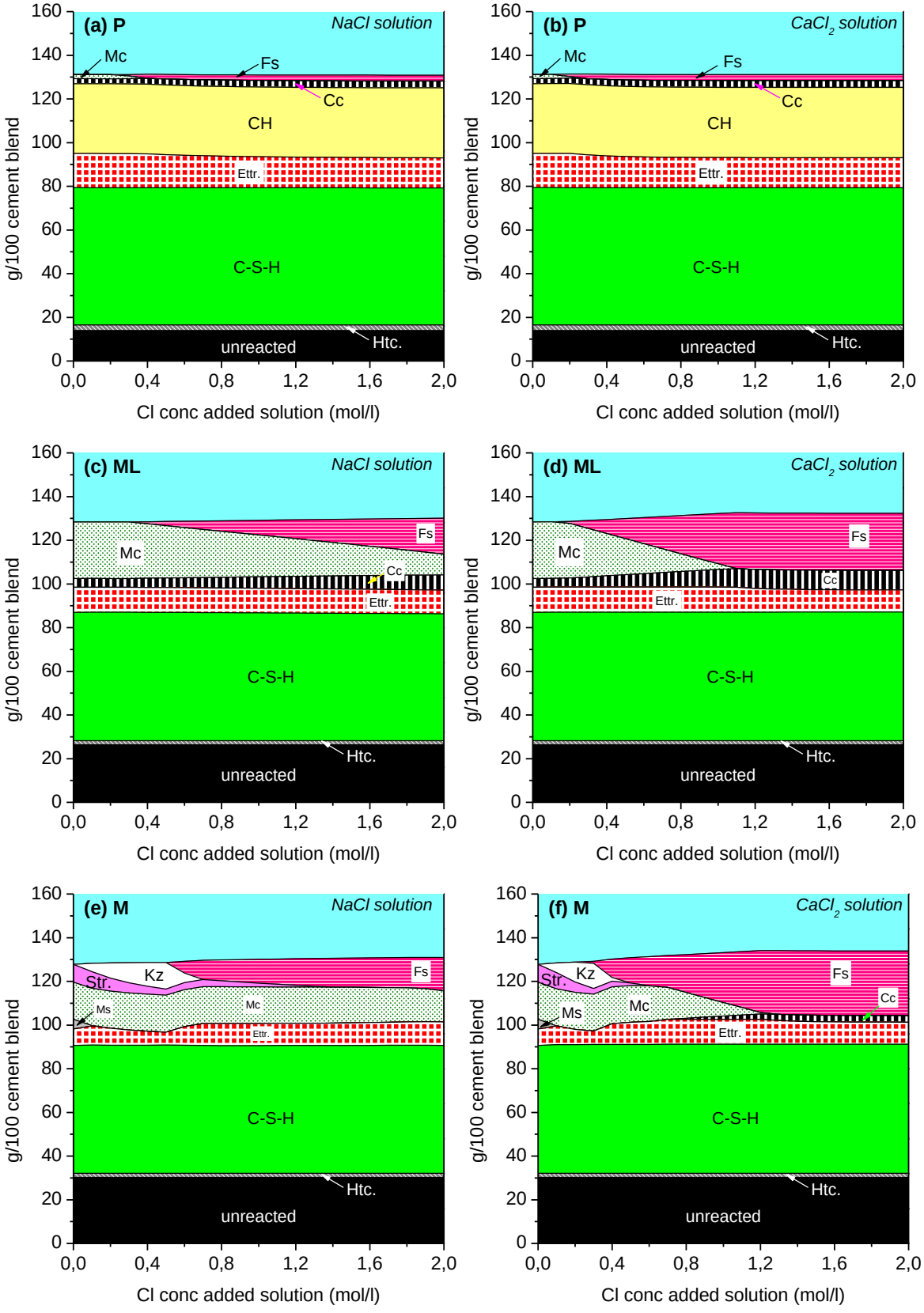

Fig. 1. Phase assemblages for the P, ML and M pastes exposed to the NaCl and $CaCl_2$ solutions. C-S-H: calcium-silicate-hydrate; Ettr.: ettringite; CH: portlandite; Mc: monocarbonate; Str.: strätlingite; Cc: $CaCO_3$; Fs: Friedel's salt; Kz: Kuzel's salt; Htc.: Hydrotalcite.

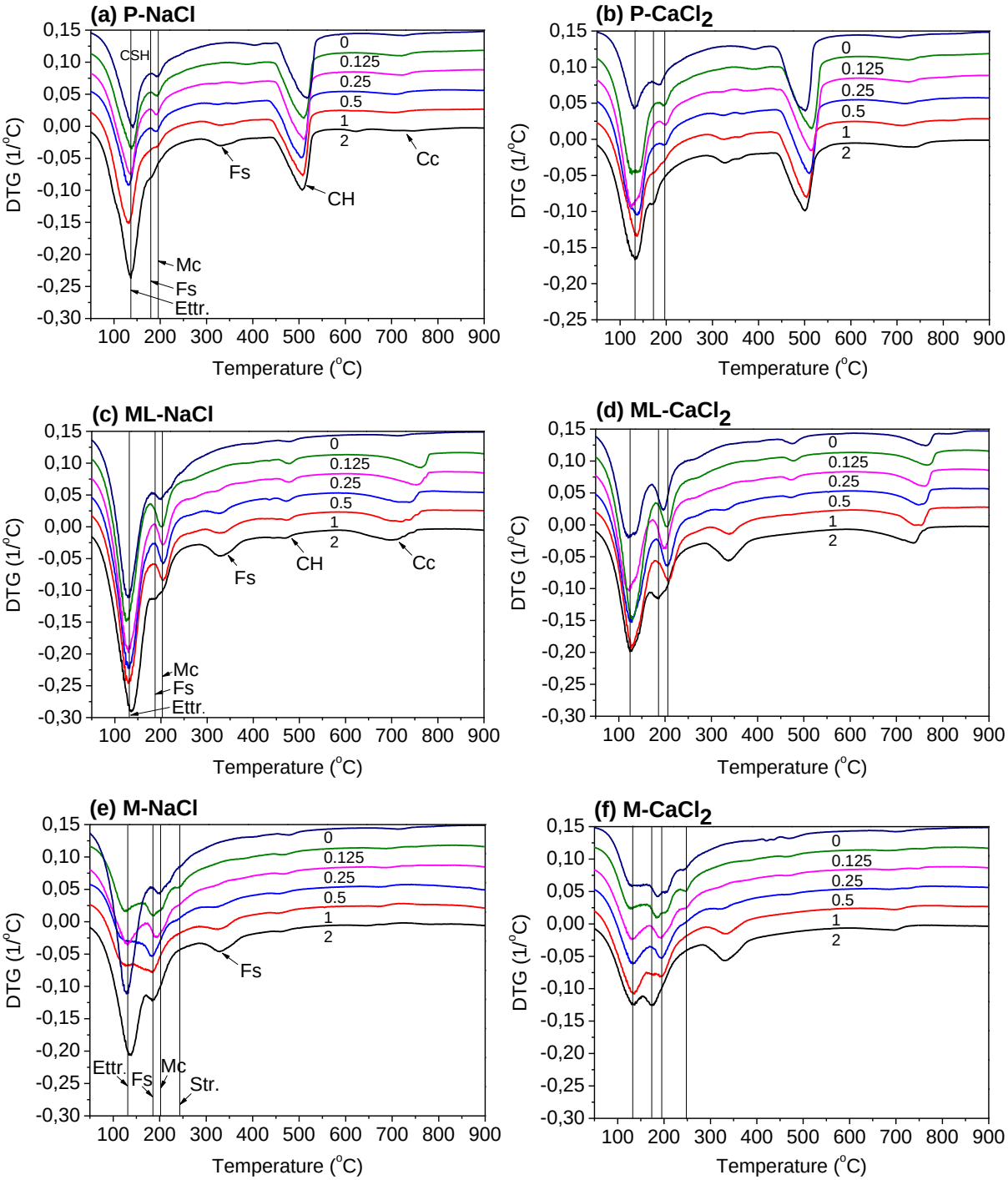

Fig. 2. DTG curves of the pastes exposed to the NaCl (a, c and e) and $CaCl_2$ (b, d and f) solutions with different chloride concentrations (0 - 2.0 mol/L). The area of the second weight loss for Friedel's salt is highlighted. CSH: calcium-silicate-hydrate; Ettr.: ettringite; Fs: Friedel's salt; Mc: monocarbonate; Str: strätlingite; CH: portlandite; Cc: calcium carbonate

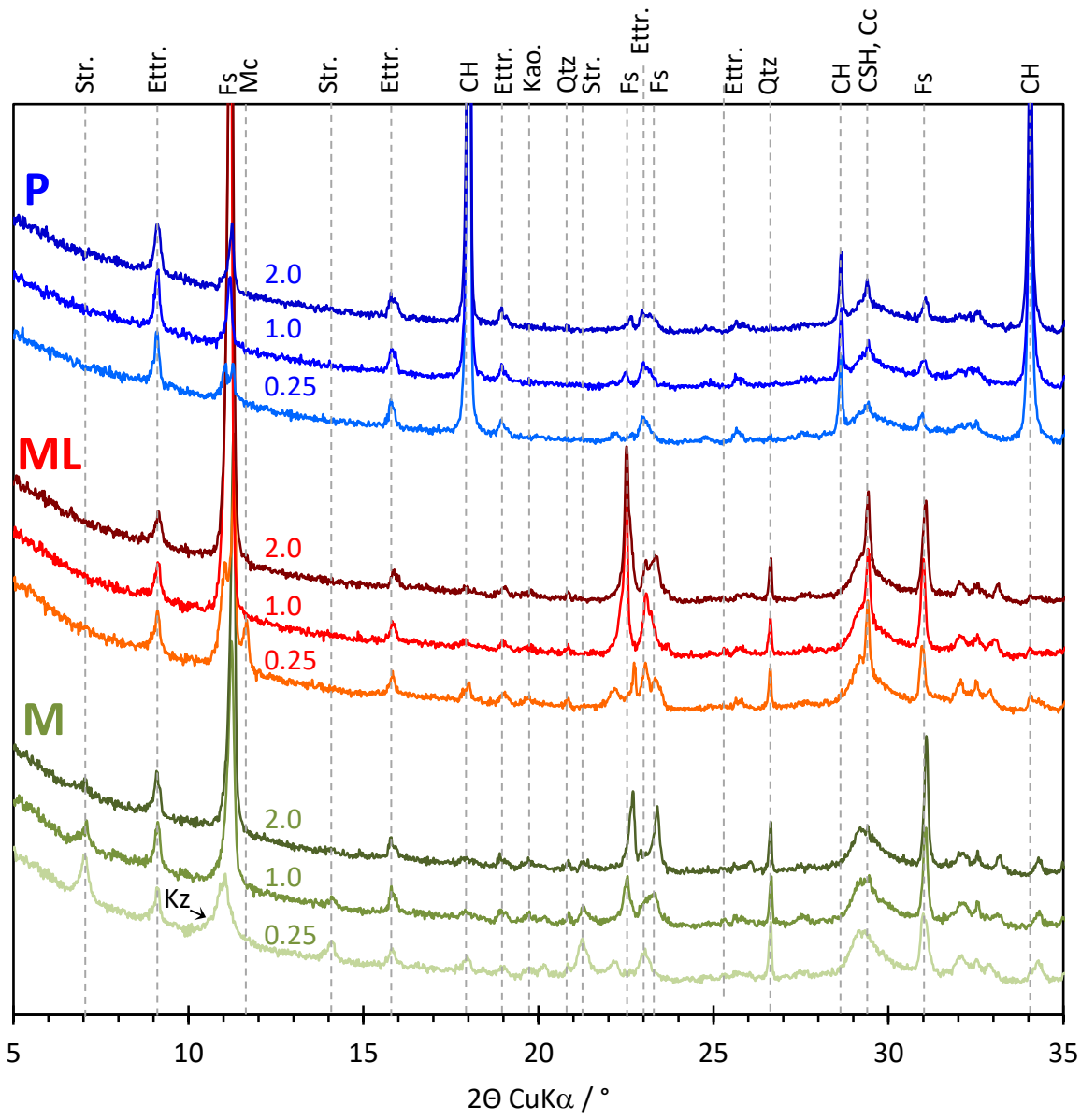

Fig. 3. XRD patterns of the pastes exposed to the $CaCl_2$ solutions with different chloride concentration (0.25, 1.0 and 2.0 mol/L). CSH: calcium-silicate-hydrate; Ettr.: ettringite; Fs: Friedel's salt; Mc: monocarbonate; Str: strätlingite; CH: portlandite; Cc: calcium carbonate; Kz: Kuzel's salt; Kao.: Kaolinite; Qtz.: Quartz.

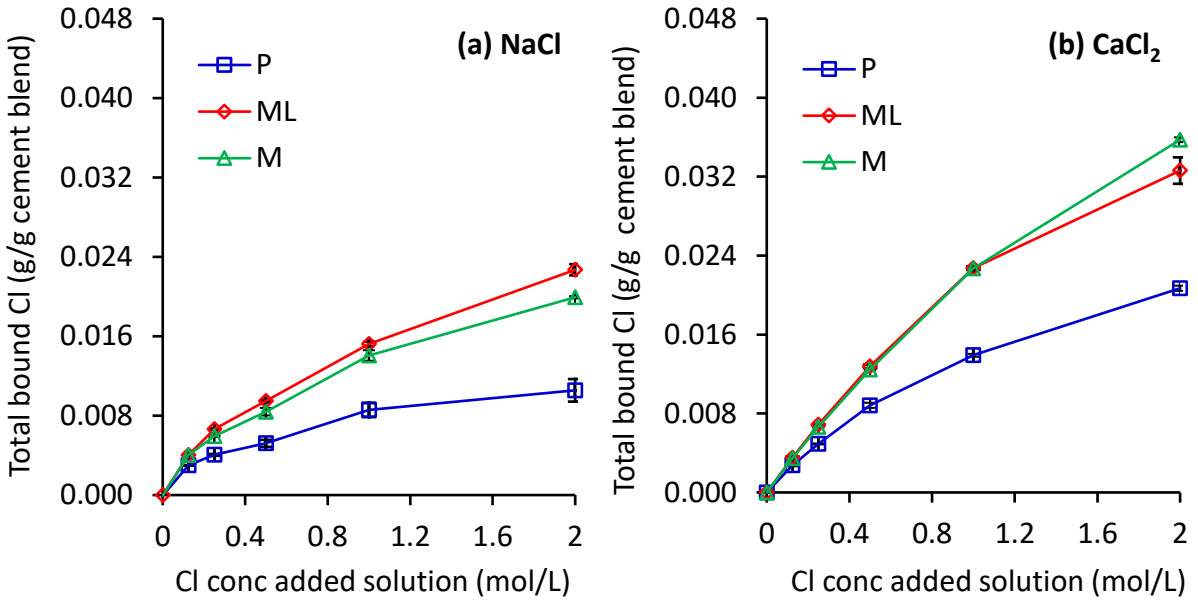

Fig. 4. Chloride binding isotherms for the P, ML and M pastes exposed to (a) NaCl and (b) $CaCl_2$ solutions. The bound chloride content is reported as g per g of unhydrated cement blend and shown as a function of the concentration of added chloride ions in the exposure solutions.

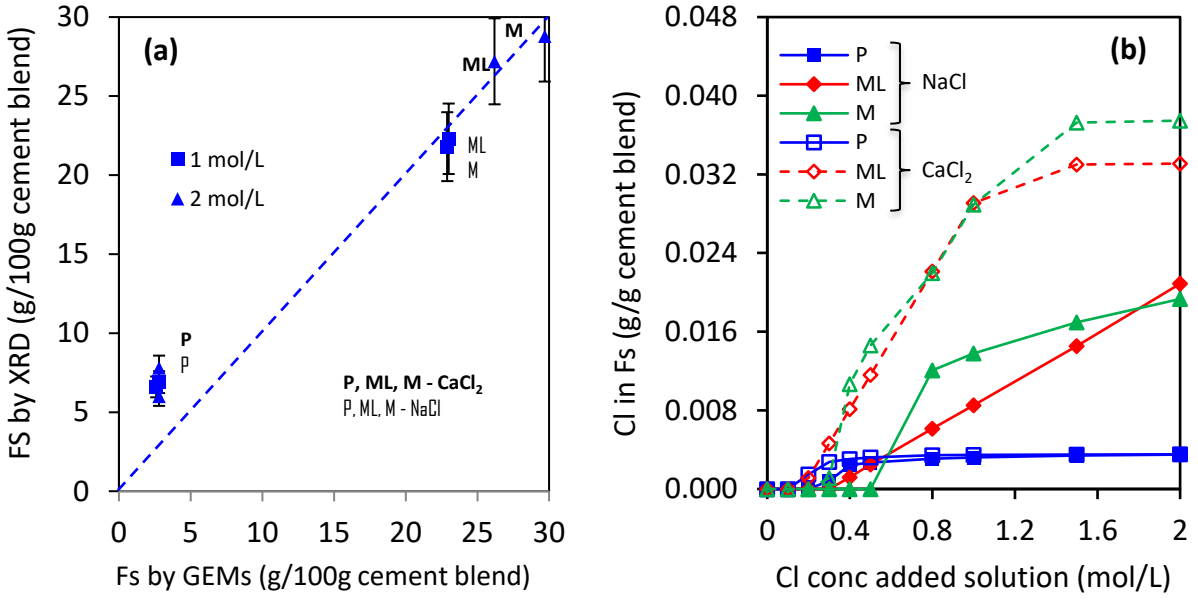

Fig. 5. Chloride bound as Friedel's salt for all the pastes exposed to the NaCl and $CaCl_2$ solutions. (a) Relationship between the calculated (by thermodynamic modeling) and measured (by XRD) amount of Friedel's salt. (b) The amount of chloride binding isotherm from Friedel's salt predicted by thermodynamic modeling.

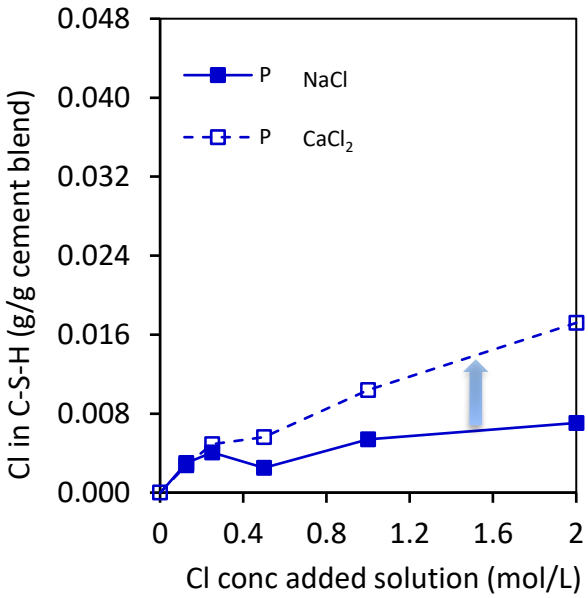

Fig. 6. Chloride absorbed on the C-S-H phase in the P pastes calculated by subtracting the bound chloride in Friedel's salt predicted by thermodynamic modeling from the total bound chloride.

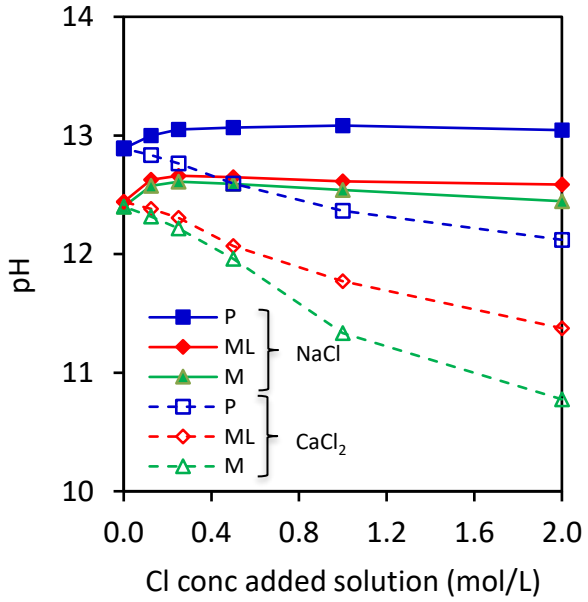

Fig. 7. pH values as a function of the chloride concentrations of the exposure solutions for the pastes exposed to the NaCl and $CaCl_2$ solutions.

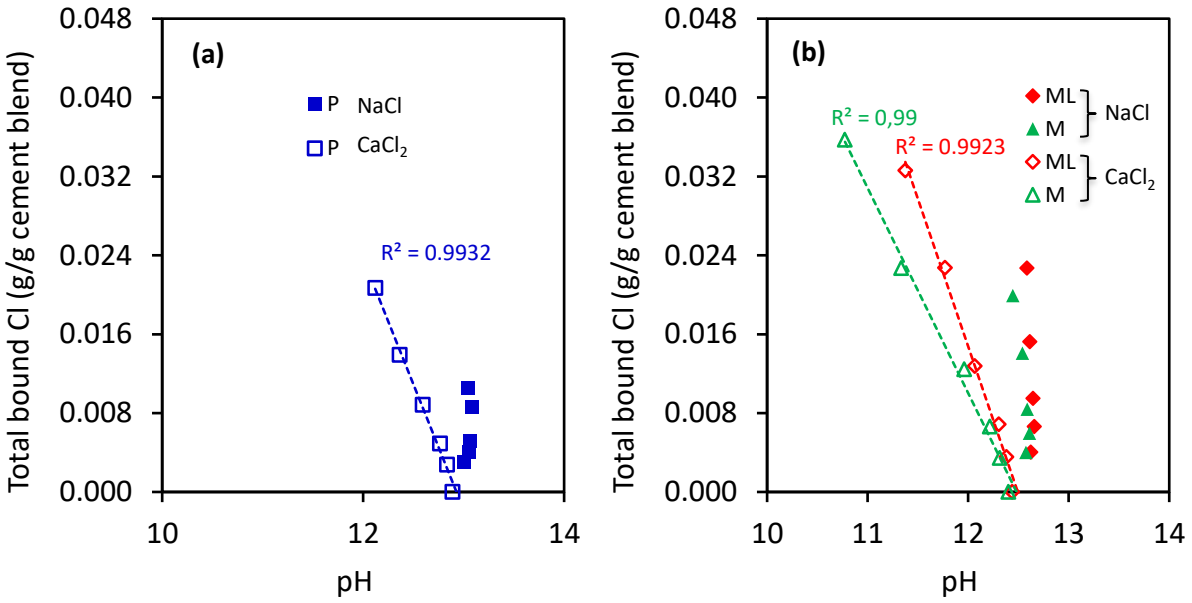

827

828 Fig. 8. Relationship between the total bound chloride and the pH of the exposure solutions for

829 (a) the P paste and (b) the ML and M pastes exposed to the NaCl and $CaCl_2$ solutions.

830

831

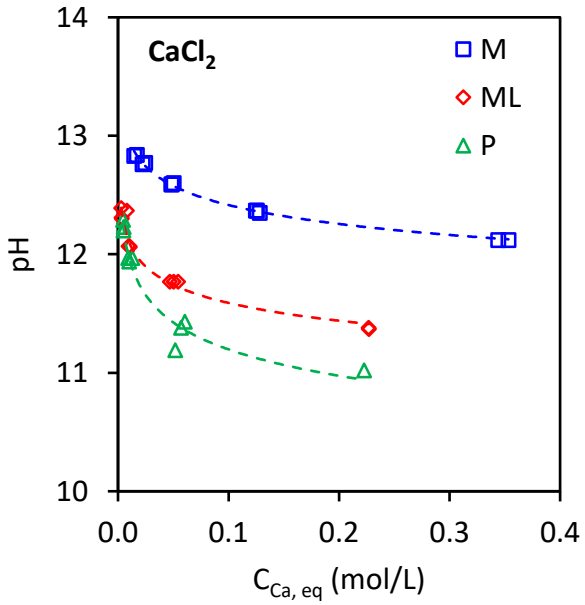

832

833 Fig. 9. Relationship between pH and the measured calcium concentration ($C_{Ca,eq}$) in the $CaCl_2$

834 exposure solution at equilibrium condition.

835

836

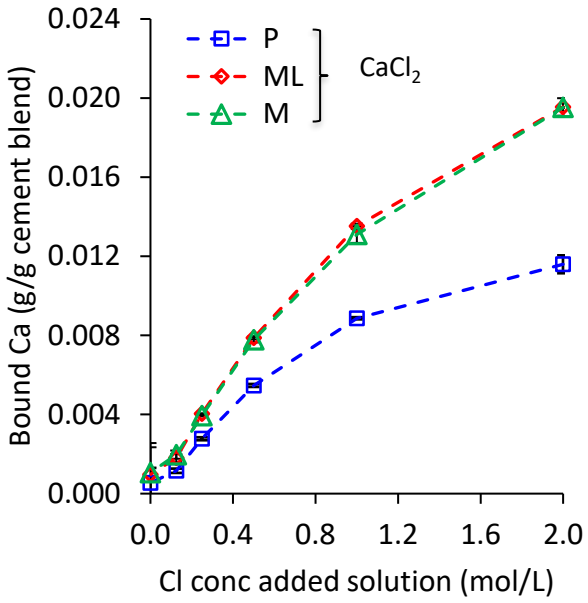

837

838

839 Fig. 10. Calcium binding isotherm (*i.e.*, uptake of calcium from the $CaCl_2$ exposure solution by

840 hydration products) for the well-hydrated P, ML and M pastes exposed to the $CaCl_2$ solution.

841

842

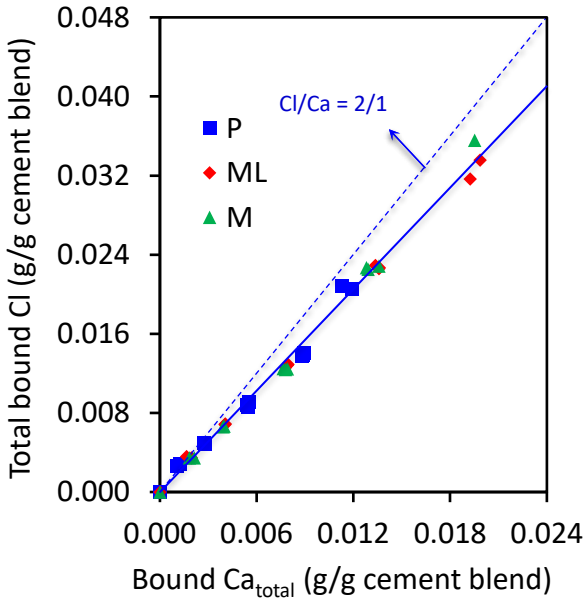

843

844

845 Fig. 11. Relationship between the total bound chloride and the total "bound" calcium (*i.e.*,

846 uptake of calcium from the $CaCl_2$ exposure solution by hydration products) for pastes exposed

847 to the $CaCl_2$ solution for pastes exposed to the $CaCl_2$ solution.

848

849

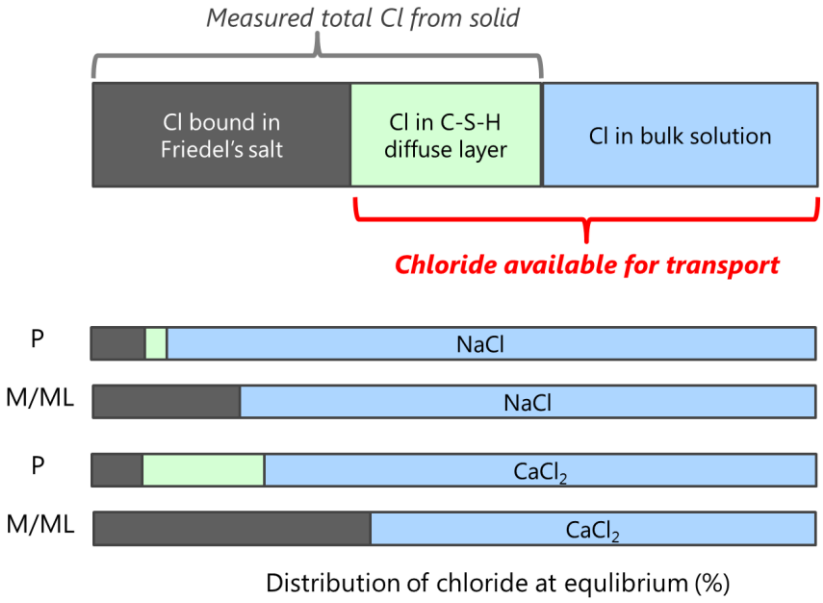

Fig. 12. Schematic description of the chloride distribution in the P, ML and M paste samples exposed to the NaCl and $CaCl_2$ solutions.